2015 IEEE International Conference on Robotics and Automation (ICRA)
Washington State Convention Center
Seattle, Washington, May 26-30, 2015

Planning the Motion of a Sliding and Rolling Sphere

Yan-Bin Jia
Department of Computer Science
Iowa State University
Ames, IA 50010, USA
jia@iastate.edu

***Abstract*— This paper investigates the free motion of a sphere with initial velocity and angular velocity on a plane under sliding and rolling friction. The sphere will first slide along a parabolic trajectory (with a constant direction of its contact velocity), and then roll along a straight trajectory. Such a curved trajectory can be utilized for obstacle avoidance in path planning. A one-to-one correspondence exists between trajectories connecting two specified locations and pairs of sliding and rolling directions within some 2-dimensional region, called the *trajectory space*, which is then used for planning. A plane sweep algorithm operating in this space is presented to find all collision-free trajectories in the presence of cylindrical obstacles that are vertically oriented.**

I. Introduction

A sphere on a plane can achieve re-orientation, that is, change the orientation of its body frame, by simply rolling on the plane. Motion planning for the sphere, called the ball-plate problem, exploits the nonholonomic rolling constraint to construct a rolling path (desirably closed) that results in some prescribed change in the sphere's orientation. A number of re-orientation algorithms [5], [7], [8], [11] have been designed using techniques from plane trigonometry or differential geometry. Spherical robots [1], [2] have also been designed to perform rolling and spinning operations in a controlled manner.

While rolling has received much attention in path planning, mobile robots, grasping, and dexterous manipulation, sliding has largely been regarded as a "negative phenomenon" to avoid, especially in the last two areas above. In this paper, we are going to demonstrate that sliding offers the benefit of curving the trajectory of a moving sphere, which can be utilized to avoid obstacles in path planning.

One motivation comes from billiard sports. The cue ball after a massé shot will initially slide along a curve, making slight noise from scratching the felt, before rolling straight ahead.

Support for this research was provided in part by Iowa State University (ISU).

II. Moving Sphere on a Plane

Figure 1 illustrates the general case of a sphere with radius ρ moving on a horizontal plane $\mathcal{P}$. The sphere

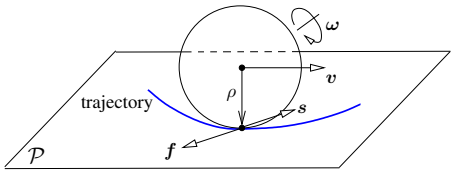

Fig. 1. Contact velocity $\boldsymbol{s}$ of a sphere and contact frictional force $\boldsymbol{f}$.

has no actuation or control during its motion, which is completely influenced by friction. Does there exist initial velocity $\boldsymbol{v}_0$ and angular velocity $\boldsymbol{\omega}_0$ that will take the sphere to some location $\boldsymbol{q}$ while avoiding obstacles?

Without loss of generality, we let the origin $\boldsymbol{o}$ be at the sphere's starting location, the x-axis point toward $\boldsymbol{q}$, and the xy-plane coincide with $\mathcal{P}$. The following two assumptions are made:

1) *There exists at least one obstacle at distance ρ or less from the line segment $\overline{\boldsymbol{oq}}$.*
2) *$\boldsymbol{v}_0$ and $\boldsymbol{\omega}_0$ have no components in the z-direction.*

If the first assumption does not hold, the line segment $\overline{\boldsymbol{oq}}$ would be a collision-free trajectory, making the problem a trivial one. The z-component of $\boldsymbol{v}_0$ is assumed to be zero to ignore bouncing of the sphere. The z-component of $\boldsymbol{\omega}_0$ plays no part in the initial velocity at the sphere's contact point with the plane, referred to as the *sliding velocity*:

$$\boldsymbol{s}_0 = \boldsymbol{v}_0 + \rho\hat{\boldsymbol{z}} \times \boldsymbol{\omega}_0 \tag{1}$$

due to the cross product with $\hat{\boldsymbol{z}} = (0, 0, 1)^T$. We shall see later in this section that $\boldsymbol{s}_0$ and $\boldsymbol{v}_0$ determine the sphere trajectory. The assumption about $\boldsymbol{\omega}_0$ will merely make our presentation clean.

A. Sliding

Sliding happens when $\boldsymbol{s}_0$ is not zero. Let the sphere have mass m. Its angular inertia matrix is equal to the

$\frac{2}{5}m\rho^2$ times the 3×3 identity matrix. Its velocity $\boldsymbol{v}$ and angular velocity $\boldsymbol{\omega}$ yield the following sliding velocity

$$\boldsymbol{s} = \boldsymbol{v} + \rho\hat{\boldsymbol{z}} \times \boldsymbol{\omega}. \tag{2}$$

The sphere is subject to a frictional force $\boldsymbol{f} = -\mu_s mg\hat{\boldsymbol{s}}$, where μ_s is the coefficient of sliding friction, $g > 0$ the magnitude of the gravitational acceleration, and $\hat{\boldsymbol{s}} = \boldsymbol{s}/\|\boldsymbol{s}\|$, the sliding direction. Working out the dynamics, we obtain the sphere's acceleration $\dot{\boldsymbol{v}} = -\mu_s g\hat{\boldsymbol{s}}$ and angular acceleration $\dot{\boldsymbol{\omega}} = \frac{5}{2\rho}\mu_s g\hat{\boldsymbol{z}} \times \hat{\boldsymbol{s}}$.

We derive the contact acceleration by differentiating (2) and substituting the expressions of $\dot{\boldsymbol{v}}$ and $\dot{\boldsymbol{\omega}}$ in:

$$\dot{\boldsymbol{s}} = -\mu_s g\hat{\boldsymbol{s}} + \tfrac{5}{2}\mu_s g\hat{\boldsymbol{z}} \times (\hat{\boldsymbol{z}} \times \hat{\boldsymbol{s}}) = -\tfrac{7}{2}\mu_s g\hat{\boldsymbol{s}}, \tag{3}$$

using $\hat{\boldsymbol{z}} \cdot \hat{\boldsymbol{s}} = 0$. The above implies that $\dot{\boldsymbol{s}}$ is opposite to $\boldsymbol{s}_0$, which further implies that $\boldsymbol{s}$ will not change its direction until it becomes to zero. We refer to $\hat{\boldsymbol{s}} = \boldsymbol{s}_0/\|\boldsymbol{s}_0\|$ as the *sliding direction*.

With $\hat{\boldsymbol{s}}$ being constant, we can integrate $\dot{\boldsymbol{s}}$, $\dot{\boldsymbol{v}}$, and $\dot{\boldsymbol{\omega}}$ to obtain $\boldsymbol{s}$, $\boldsymbol{v}$, and $\boldsymbol{\omega}$, as derived earlier in [6, pp. 10–11]. The sliding trajectory is obtained from one more round of integration — this time of $\boldsymbol{v}$:

$$\boldsymbol{x} = (x, y)^T = \boldsymbol{v}_0 t - \tfrac{1}{2}\mu_s g\hat{\boldsymbol{s}}t^2, \qquad 0 \le t \le t_r. \tag{4}$$

Sliding ends (i.e., $\boldsymbol{s} = 0$) at time $t_r = 2\|\boldsymbol{s}_0\|/(7\mu_s g)$ with velocity and location given by

$$\boldsymbol{v}_r = \boldsymbol{v}_0 - \mu_s g \cdot t_r\hat{\boldsymbol{s}} = \boldsymbol{v}_0 - \tfrac{2}{7}\boldsymbol{s}_0, \tag{5}$$

$$\boldsymbol{x}_r = \boldsymbol{x}(t_r) = \left(\boldsymbol{v}_0 - \tfrac{1}{7}\boldsymbol{s}_0\right) t_r. \tag{6}$$

B. Pure Rolling

At time t_r, $\boldsymbol{v}_r$ is found orthogonal to the angular velocity $\boldsymbol{\omega}_r$, after taking cross product of $\boldsymbol{v}$ with (2) under $\boldsymbol{s} = 0$. The frictional force opposes the direction of $\boldsymbol{v}_r$. Neither $\boldsymbol{\omega}$ nor $\boldsymbol{v}$ will change its direction from t_r on. The sphere starts pure rolling without slip ($\boldsymbol{s} = 0$).

The rolling trajectory is a straight line segment. To derive the deceleration of the sphere, we adopt Marlow's treatment [6, p. 12] based on the principle of energy dissipation. Because the sphere rolls on a line, we can now denote $\boldsymbol{v}$ and $\boldsymbol{\omega}$ by their magnitudes v and ω with no ambiguity. Since $v = \rho\omega$ under pure rolling, the kinetic energy of the sphere is

$$E = \tfrac{1}{2}mv^2 + \tfrac{1}{2} \cdot \left(\tfrac{2}{5}m\rho^2\right)\omega^2 = \tfrac{7}{10}mv^2.$$

Its dissipation rate $\dot{E}$ under rolling friction equals $-\mu_r mgv$. From this, we can show that the sphere will come to stop at time $t_e = t_r + 7\|\boldsymbol{v}_r\|/(5\mu_r g)$, along the following line trajectory trajectory of rolling:

$$\boldsymbol{x} = \boldsymbol{x}_r + \boldsymbol{v}_r(t - t_r) - \tfrac{5}{14}\mu_r g\hat{\boldsymbol{r}}(t - t_r)^2, \tag{7}$$

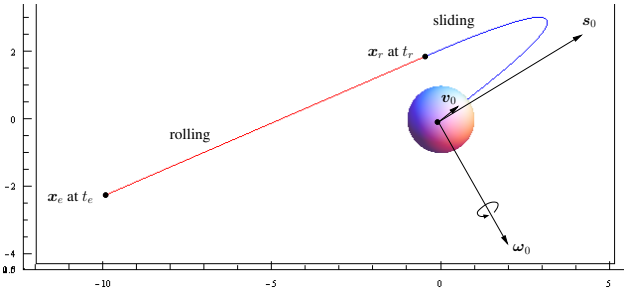

Fig. 2. Trajectory of a sphere with unit radius, initial velocities $\boldsymbol{v}_0 = (4, 3)^T$ and $\boldsymbol{\omega}_0 = (14, -25)^T$, which yield initial sliding velocity $\boldsymbol{s}_0 = (29, 17)^T$. The velocities are drawn as arrows of lengths proportional to their magnitudes. Rolling starts at $\boldsymbol{x}_r = (-0.466687, 1.86675)^T$ at time $t_r = 3.26681$ and ends at $\boldsymbol{x}_e = (-9.99892, -2.26389)^T$ at time $t_e = 7.71519$. The coefficients of friction are $\mu_s = 0.3$ and $\mu_r = 0.5$.

$t_r < t \le t_e$, where $\hat{\boldsymbol{r}} = \boldsymbol{v}_r/\|\boldsymbol{v}_r\|$ is the *rolling direction*. The sphere will be resting at the location

$$\boldsymbol{x}_e = \boldsymbol{x}(t_e) = \boldsymbol{x}_r + (7\|\boldsymbol{v}_r\|/(10\mu_r g))\boldsymbol{v}_r. \tag{8}$$

Equations (4) and (7) together describe the sphere trajectory. An example is shown in Fig. 2.[1]

III. Trajectories to Destination

It is not difficult to show that $\boldsymbol{v}_0 \cdot \boldsymbol{\omega}_0 = 0$ results in a straight sliding trajectory, using (1) and (4). Under Assumption 1, a straight trajectory would result in collision with some obstacle. Therefore, the case $\boldsymbol{v}_0 \cdot \boldsymbol{\omega}_0 = 0$ will not be considered from now on.

Theorem 1: When $\boldsymbol{v}_0 \cdot \boldsymbol{\omega}_0 \neq 0$, the sphere slides along a parabola generated from first rotating $y = \frac{1}{2}\left(\mu_s g/\|\boldsymbol{v}_0 \times \hat{\boldsymbol{s}}\|^2\right) x^2$ about the origin through $\phi + \pi/2$, where $\hat{\boldsymbol{s}} = \binom{\cos\phi}{\sin\phi}$, and then translating it by $\boldsymbol{x}^* = (\boldsymbol{v}_0 \cdot \hat{\boldsymbol{s}}/(\mu_s g))\left(\boldsymbol{v}_0 - \frac{1}{2}(\boldsymbol{v}_0 \cdot \hat{\boldsymbol{s}})\hat{\boldsymbol{s}}\right)$.

Due to limited space, the proof of the theorem is omitted, as will those of other proposition and theorems in this paper. As an example, the sphere trajectory in Fig. 2 is a parabola $y = 4.60139x^2$ undergoing a rotation through the angle 2.10101 and then a translation by $(3.13805, 2.94665)^T$.

We would like to describe the set of velocities $(\boldsymbol{v}_0, \boldsymbol{\omega}_0)$ that will take the sphere to rest at a given location $\boldsymbol{x}_e = \boldsymbol{q}$. By rewriting (1) and (5) into a matrix equation, the pair $(\boldsymbol{s}_0, \boldsymbol{v}_r)$ of initial sliding and rolling velocities has a one-to-one correspondence to $(\boldsymbol{v}_0, \rho\hat{\boldsymbol{z}} \times \boldsymbol{\omega}_0)$, the second element of which in turn has a one-to-one correspondence to $\boldsymbol{\omega}_0$ under Assumption 2 and $\boldsymbol{v}_0 \cdot \boldsymbol{\omega}_0 \neq 0$. Thus, we need only consider $(\boldsymbol{s}_0, \boldsymbol{v}_r)$.

[1]From now on, the sliding segment of a trajectory will be drawn in blue, and the rolling segment will be drawn in red.

Next, plug $\boldsymbol{v}_0 = \frac{2}{7}\boldsymbol{s}_0 + \boldsymbol{v}_r$, obtained from (5), into (6) and the result into (8) to rewrite $\boldsymbol{q} = c_s\hat{\boldsymbol{s}} + c_r\hat{\boldsymbol{r}}$, where c_s and c_r are non-negative expressions in terms of $\|\boldsymbol{s}_0\|$ and $\|\boldsymbol{v}_r\|$.

Proposition 2: There exist $\boldsymbol{v}_0$ and $\boldsymbol{\omega}_0$ with $\boldsymbol{v}_0 \cdot \boldsymbol{\omega}_0 \neq 0$ that will take the sphere to a stop at $\boldsymbol{q}$ if and only if the cone spanned by $\hat{\boldsymbol{s}}$ and $\hat{\boldsymbol{r}}$ contains $\boldsymbol{q}$ in its interior.

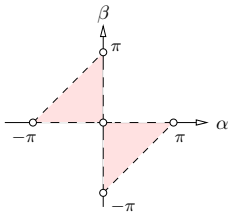

Fig. 3. C-space of trajectories $\mathcal{T}(\alpha, \beta)$ that take the sphere from the origin to a point on the positive x-axis. The space consists of two open triangular regions bounded by the two axes and the lines $\alpha - \beta = \pi$ and $\beta - \alpha = \pi$.

The unit vectors $\hat{\boldsymbol{s}}$ and $\hat{\boldsymbol{r}}$ are respectively determined by their polar angles α and β, referred to as the *sliding angle* and *rolling angle*. We can reconstruct the initial velocities $\boldsymbol{v}_0$ and $\boldsymbol{\omega}_0$ (and thus the trajectory) from α and β when the cone spanned by $\hat{\boldsymbol{s}}$ and $\hat{\boldsymbol{v}}$ contains $\boldsymbol{q}$ in the interior. It can be shown that the correspondence thus defined between (α, β) and $(\boldsymbol{v}_0, \boldsymbol{\omega}_0)$ is one-to-one. Nevertheless, the forms of $\boldsymbol{v}_0$ and $\boldsymbol{\omega}_0$ in terms of α and β are too complicated with sines, cosines, and square roots to be up for an analysis.

Denote by $\mathcal{T}(\alpha, \beta)$ the trajectory from $\boldsymbol{o}$ to $\boldsymbol{q}$ determined by α and β. Since the trajectory is a parabolic segment followed by a tangent line segment, it is convex and thus either above the x-axis or below it except at $\boldsymbol{o}$ and $\boldsymbol{q}$. Under Proposition 2, we infer that to reach $\boldsymbol{q}$ all feasible (α, β) form the following set:

$$D = (0, \pi) \times (\alpha - \pi, 0) \cup (-\pi, 0) \times (0, \alpha + \pi). \quad (9)$$

Plotted in Fig. 3, D is the configuration space (or C-space) of trajectories, referred to as the *trajectory space*.

Theorem 3: For any $(\alpha, \beta) \in D$, $\mathcal{T}(\alpha, \beta)$ and $\mathcal{T}(-\alpha, -\beta)$ are reflections of each other in the x-axis.

Let $\mathcal{R}_o$ and $\mathcal{R}_q$ be the two rays originating respectively from $\boldsymbol{o}$ and $\boldsymbol{q}$ in the direction $\hat{\boldsymbol{s}}$, and $\mathcal{R}'_o$ and $\mathcal{R}'_q$ be the two rays originating respectively from $\boldsymbol{o}$ and $\boldsymbol{q}$ in the direction $-\hat{\boldsymbol{r}}$.

Theorem 4: For a fixed sliding angle $\alpha \in (0, \pi)$, the following statements hold:

i) For any two rolling angles $\beta_1, \beta_2 \in (\alpha - \pi, 0)$ with $\beta_2 < \beta_1$, except at $\boldsymbol{o}$ and $\boldsymbol{q}$, $\mathcal{T}(\alpha, \beta_1)$ lies inside the region bounded by $\mathcal{T}(\alpha, \beta_2)$ and $\overline{\boldsymbol{oq}}$.
ii) Every point $\boldsymbol{p}$ in the interior of the region bounded by $\overline{\boldsymbol{oq}}$, $\mathcal{R}_o$, and $\mathcal{R}_q$ lies on exactly one trajectory $\mathcal{T}(\alpha, \beta)$, $\beta \in (\alpha - \pi, 0)$.

Theorem 5: For a fixed rolling angle $\beta \in (-\pi, 0)$, the following statements hold:

i) For any two sliding angles $\alpha_1, \alpha_2 \in (0, \beta + \pi)$ with $\alpha_1 < \alpha_2$, except at $\boldsymbol{o}$ and $\boldsymbol{q}$, $\mathcal{T}(\alpha_1, \beta)$ lies inside the region bounded by $\mathcal{T}(\alpha_2, \beta)$ and $\overline{\boldsymbol{oq}}$.
ii) Every point $\boldsymbol{p}$ in the interior of the region bounded by $\overline{\boldsymbol{oq}}$, $\mathcal{R}'_o$, and $\mathcal{R}'_q$ lies on exactly one trajectory $\mathcal{T}(\alpha, \beta)$, $\alpha \in (0, \beta + \pi)$.

Fig. 4 plots two groups of trajectories respectively with the same sliding and rolling angles. The values

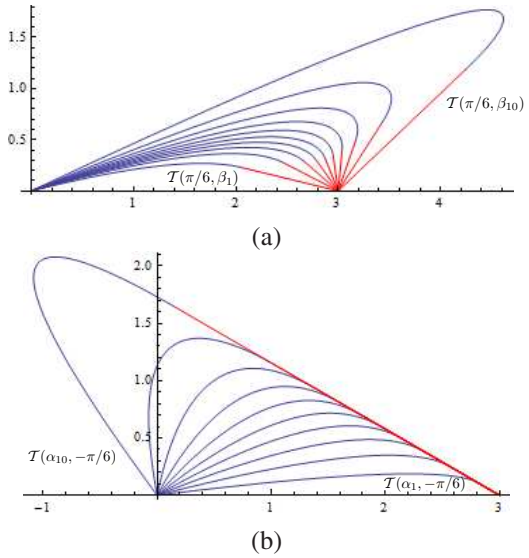

Fig. 4. Two groups of 10 trajectories each from the origin to $(3, 0)$ with (a) the same sliding angle $\alpha = \pi/6$ but different rolling angles $\beta_i = -\frac{i}{11}(\pi - \alpha)$, $1 \leq i \leq 10$; and (b) the same rolling angle $\beta = -\pi/6$ but different sliding angles $\alpha_i = \frac{i}{11}(\beta + \pi)$, $1 \leq i \leq 10$.

$\mu_s = 0.3$ and $\mu_r = 0.15$ of the coefficients of friction will also be used in the remaining examples in the paper.

IV. Motion Planning

According to Theorem 3, we need only consider how to find a collision-free path from $\boldsymbol{o}$ to $\boldsymbol{q}$ that goes above the x-axis. Such a path is represented by a point in the lower triangular region D^- in Fig. 3. This implies that we need only consider obstacles that are above or intersected by the x-axis. To find the trajectory below the x-axis, simply reflect all obstacles in the x-axis, invoke the algorithm and then reflect the found path in the x-axis again.

To simplify, obstacles are vertical line segments standing on the xy-plane at the points $\boldsymbol{b}_1, \ldots, \boldsymbol{b}_n$ and having length at least the radius ρ of the sphere. In the C-space for path planning, the sphere shrinks to a point, and every obstacle induces a disk $\mathcal{C}_i$ at $\boldsymbol{b}_i$ of radius ρ. The disk is a C-space obstacle referred to as a *C-circle*.

A. Constraint Curves in the C-Space of Trajectories

Every C-circle $\mathcal{C}_i$ defines some region in the trajectory space D^- that includes all the trajectories which would collide with the obstacle $\boldsymbol{b}_i$. Such a region is bounded by curves on which every point (α, β) yields a trajectory $\mathcal{T}(\alpha, \beta)$ tangent to $\mathcal{C}_i$.

The obstacles not below the x-axis are either A) above the x-axis; or intersecting the x-axis B) between $\boldsymbol{o}$ and $\boldsymbol{q}$, C) to the left of $\boldsymbol{o}$, or D) to the right of $\boldsymbol{q}$.

1) Type A Obstacle: To simplify notation, we refer to $\boldsymbol{b}_i$ as $\boldsymbol{b}$ and $\mathcal{C}_i$ as $\mathcal{C}$. There exist two groups of tangent trajectories: those that bound $\mathcal{C}$ from above and those that bound it from below. To characterize them, we note that there are two tangent lines from $\boldsymbol{o}$ to $\mathcal{C}$ at $\boldsymbol{p}_o^+$ from the above and at $\boldsymbol{p}_o^-$ from the below. Similarly, the two tangent lines from $\boldsymbol{q}$ to $\mathcal{C}$ has tangencies $\boldsymbol{p}_q^+$ and $\boldsymbol{p}_q^-$.

Every upper-bounding tangent trajectory has a tangency point between $\boldsymbol{p}_o^+$ and $\boldsymbol{p}_q^+$ on $\mathcal{C}$. As illustrated in Fig. 5(a), the maximum β value, denoted $\beta^+_{\max}$, is the polar angle of the vector $\boldsymbol{q} - \boldsymbol{p}_q^+$. From Fig. 3, $\alpha \leq \beta_{\max} + \pi \equiv \alpha_{\max}$. Meanwhile, the α value of the trajectory must be bounded from below by the polar angle of $\boldsymbol{p}_o^+$, denoted $\alpha^+_{\min}$. As α increases from $\alpha^+_{\min}$ (exclusive), the tangent trajectory $\mathcal{T}(\alpha, \beta)$ will have β increase from $\alpha^+_{\min} - \pi$ (exclusive). This is the case with $\mathcal{T}_1$ in Fig. 5(a). Eventually, α will increase to a value α^+_{mid} where the sphere starts rolling right at $\boldsymbol{p}_q^+$, as in the case of $\mathcal{T}_2 = \mathcal{T}(\alpha^+_{\text{mid}}, \beta^+_{\text{mid}})$ in the figure. As α continues to increase, the β value will stay at β^+_{mid}, which is the case of $\mathcal{T}_3$.

All (α, β) values, where $\mathcal{T}(\alpha, \beta)$ is an upper-bounding tangent trajectory form the curve $\boldsymbol{\gamma}^+$ in $\mathcal{D}^-$ plotted in Fig. 5(c). The interior of the region bounded by the curve and the line $\alpha - \beta = \pi$ includes all trajectories that will enclose the obstacle $\boldsymbol{b}$.

The second group of tangent trajectories bound the obstacle from below, as illustrated in Fig. 5(b). All such tangent trajectories are represented by the curve $\boldsymbol{\gamma}^-$ in Fig. 5(c). The interior of the region in D^- bounded by the curve and the α- and β-axes represent all collision-free trajectories below the obstacle. The shaded region in Fig. 5(c) includes all trajectories that will collide with $\boldsymbol{b}$.

2) Type B Obstacle: The portion of the C-circle above the x-axis introduces a constraint curve in D^- like $\boldsymbol{\gamma}^+$ in Fig. 5(c). Collision-free trajectories are represented by the open region enclosed by the curve and the line $\alpha - \beta = \pi$.

3) Type C and D Obstacles: Constraint curves induced by obstacles of these two types are very similar with differences in their locations in $\mathcal{D}^-$. We discuss a type D obstacle but will present a type C one later.

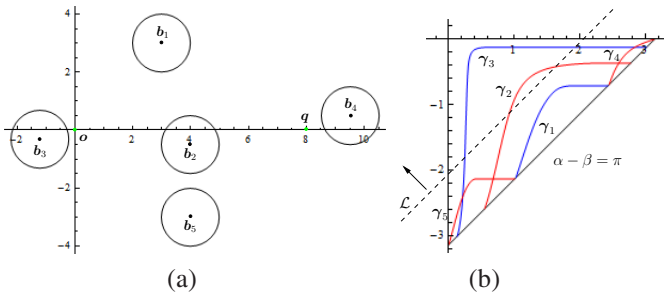

(a) (b)

Fig. 6. (a) Work space for a unit sphere moving from $\boldsymbol{o}$ to $\boldsymbol{q} = (8, 0)$ with five obstacles: $\boldsymbol{b}_1 = (3, 3)$, $\boldsymbol{b}_2 = (4, -1/2)$, $\boldsymbol{b}_3 = (-12, -3/10)$, $\boldsymbol{b}_4 = (19/2, 1/2)$, and $\boldsymbol{b}_5 = (4, -3)$, which are shown as the centers of C-space disks of radius 1. (b) Configuration space including five constraint curves induced by $\boldsymbol{b}_k$, $1 \leq k \leq 4$. The blue curves $\boldsymbol{\gamma}_1$ and $\boldsymbol{\gamma}_3$ allow points α, β (i.e., $\mathcal{T}(\alpha, \beta)$ not colliding their defining obstacles) below them. The red curves $\boldsymbol{\gamma}_2$, $\boldsymbol{\gamma}_4$, and $\boldsymbol{\gamma}_3$ allow points above them. Also shown in (b) is a sweep line $\mathcal{L}$.

Fig. 5(d) shows the same destination $\boldsymbol{q}$ with a type D obstacle at $(\frac{19}{2}, \frac{1}{2})$. Here, $\boldsymbol{p}_q$ is the point of tangency from $\boldsymbol{q}$ on the C-circle that is above the x-axis. It is easy to see that any tangent trajectory $\mathcal{T}(\alpha, \beta)$ must have $\beta \leq \beta_{\max}$, the polar angle of $\boldsymbol{q} - \boldsymbol{p}_q$. As α increases from 0^+, the point of tangency moves from infinitely close to $\boldsymbol{p}_x$, where the circle intersects the x-axis, to $\boldsymbol{p}_q$ (e.g., the trajectory $\mathcal{T}_1$). The trajectory $\mathcal{T}_2 = \mathcal{T}(\alpha_{\min}, \beta_{\min})$ starts rolling at $\boldsymbol{p}_q$. From that point, β stops changing as for the trajectory $\mathcal{T}_3$, while α increases to $\beta_{\max} + \pi$. The constraint curve is shown in Fig. 5(e).

Theorem 6: A constraint curve starts and ends on the line $\alpha - \beta = \pi$ with α increasing monotonically and β non-decreasing.

In the trajectory space $\mathcal{D}^-$, let us refer "left ", "right", "below", and "above" to the directions of the vectors $(1, 1)$, $(-1, -1)$, $(-1, 1)$, and $(1, -1)$, respectively.

B. Configuration Space

Fig. 6(a) shows an example with five obstacles. The obstacles $\boldsymbol{b}_1$ and $\boldsymbol{b}_4$ are exactly the same as in Fig. 5(a) and (d). The obstacle $\boldsymbol{b}_5$ is below the origin and eliminated when planning trajectories above the x-axis. The other four obstacles are of types A, B, C, and D, respectively. Fig. 6(b) plots the constraint curves $\boldsymbol{\gamma}_j$, $1 \leq j \leq 5$. The first two of which are induced by $\boldsymbol{b}_1$, and for $2 \leq k \leq 4$, $\boldsymbol{\gamma}_{k+1}$ is induced by $\boldsymbol{b}_k$.

The constraint curves partition $\mathcal{D}^-$ into open regions. Every point (α, β) from the same region violate the same set of constraints (i.e., $\mathcal{T}(\alpha, \beta)$ collides with the same set of obstacles). The planning problem has a solution if and only if there exists at least one open region that violates no constraint at all.

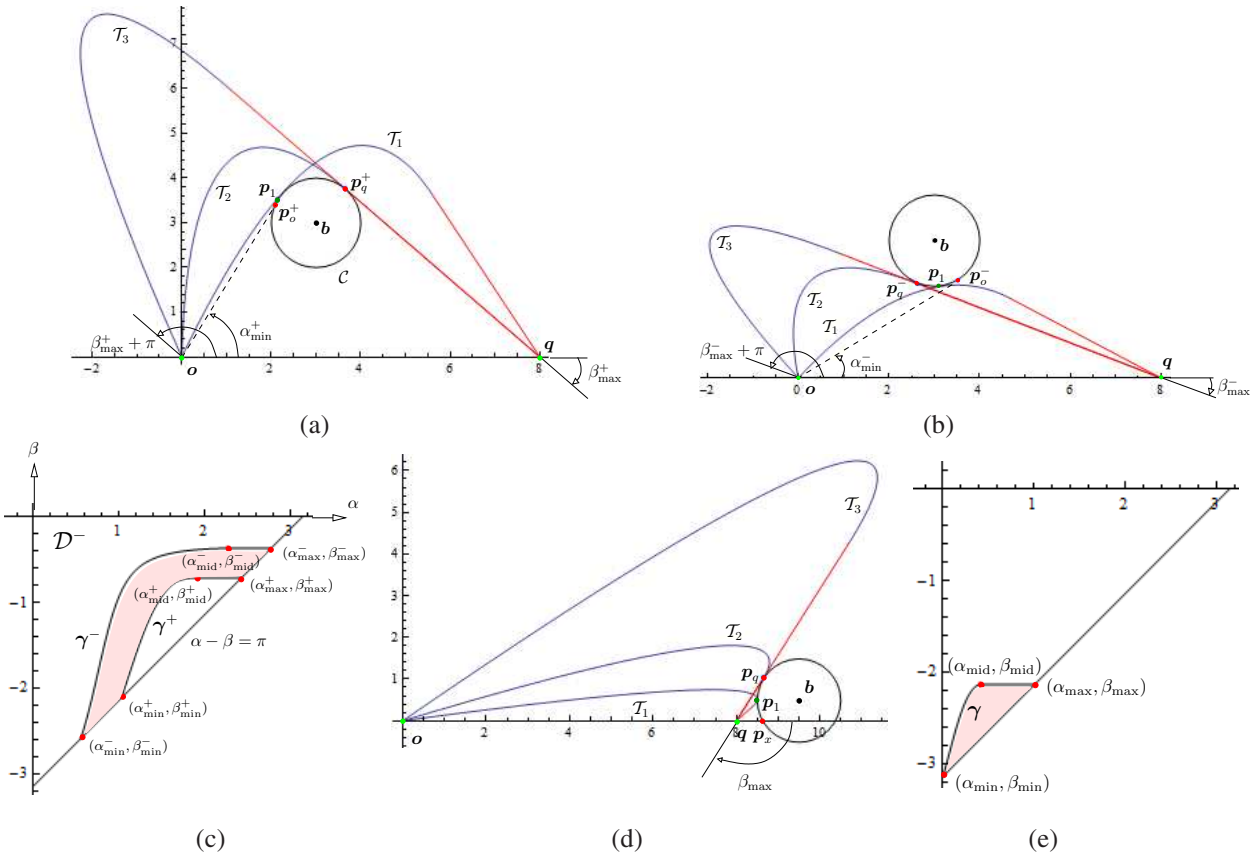

Fig. 5. Tangent trajectories and C-space obstacles ($\rho = 1$). (a) Three tangent trajectories enclosing an obstacle disk of type A at $(3, 3)$. (b) Three tangent trajectories below the disk. (c) In the C-space, the curve $\boldsymbol{\gamma}^+$ represents the set of all tangent and enclosing trajectories and the curve $\boldsymbol{\gamma}^-$ represents the set of all tangent and non-enclosing trajectories. Note that $\beta^+_{\text{mid}} = \beta^+_{\text{max}}$ and $\beta^-_{\text{mid}} = \beta^-_{\text{max}}$. (d) Tangent trajectories to an obstacle of Type D at $(19/2, 1/2)$. (e) Constraint curve induced by the obstacle in (d) in the domain $\mathcal{D}^-$. The shaded regions in (c) and (e) represent all trajectories respectively colliding with the two obstacles.

C. Plane Sweeping

We employ a plane sweep technique from computational geometry [3]. A line $\mathcal{L}$ initially aligned with $\alpha - \beta = \pi$ will sweep across D^-, handling events at stops during the sweep.

At an intermediate position, the line $\mathcal{L}$ is partitioned into segments by the constraint curves. Its *status* is a list of constraint curves ordered along the sweep line, starting with the β-axis and ending with the α-axis. Each curve has a superscript '$-$' or '$+$' to indicate that points to the left or right of the curve yield trajectories not colliding with the curve's defining obstacle. When intersected by $\mathcal{L}$, a constraint curve appears twice in the status with different superscripts.

The sweep line status is stored in a data structure such as a red-black tree [4] or a splay tree [10]. Denote by s_i the ith segment from left to right on the sweep line. An array $c[\,]$ is used such that the entry $c[i]$ counts the obstacles *colliding* with the trajectory defined by any point in the region immediately above s_i.

D. Event Handling

An event happens when the sweep line passes by either an intersection point of two constraint curves or a point on some constraint curve that is the closest to the origin. A dynamically updated event queue Q orders events in the increasing distance of the event point to the line $\alpha - \beta = \pi$.

Suppose the segment s_k on $\mathcal{L}$ at its current position is bounded by the curve $\boldsymbol{\gamma}^a_l$ on the left and the curve $\boldsymbol{\gamma}^b_r$ on the right. After the intersection, the segment s_k will be bounded by $\boldsymbol{\gamma}^b_r$ on the left and $\boldsymbol{\gamma}^a_l$ on the right. One of the following updates is performed based on (a, b):

- $(-,+)$: $c[k] \leftarrow c[k] - 2$.
- $(+,-)$: $c[k] \leftarrow c[k] + 2$.
- $(-,-)$: no change to $c[k]$.
- $(+,+)$: no change to $c[k]$.

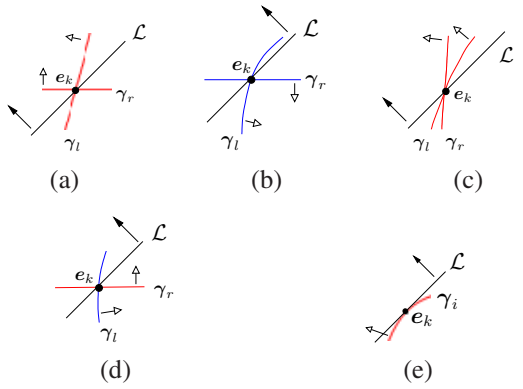

Fig. 7. Four types of intersection points: (a) $(-,+)$, (b) $(+,-)$, (c) $(-,-)$, and (d) $(+,+)$, and (e) an extremum point. A solid arrow shows the sweeping direction, while a hollow arrow marks the side where points define trajectories not in collision with the obstacle associated with the curve.

See Fig. 7 (a)–(d).

Since γ_l^a and γ_r^b have switched their order in the sweep line status, their neighboring curves in the status change. We need to check whether γ_r will intersect its new preceding curve and whether γ_l will intersect its new succeeding curve in the sweep line status. Whenever an intersection exists, add its computed position (along with the two curves) to the event queue Q.

A segment s_k on $\mathcal{L}$ bounded by the same curve γ_i may shrink to one extreme point on it. When this happens, we locate the two adjacent segments s_{k-1} and s_{k+1}, and merge them together with s_k into one bounded by the left bounding curve of s_{k-1} and the right bounding curve of s_{k+1}. No update on $c[k-1]$ needs to be done. Check if these two curves will intersect. If so, add the intersection to the queue Q.

If $c[k] = 0$, the region immediately above s_k will be a collision-free one. The entire region can be traced out as the sweep continues using a doubly-connected edge list [3, pp. 29–33].

E. Initialization

At the beginning, the sweep line coincides with the line $\alpha - \beta = \pi$. For each constraint curve, we compute its extremum point and insert it into the event queue Q.

Every constraint curve yields two entries in the sweep line status respectively associated with its two endpoints. In the ordering, complications arise with multiple obstacles of type C or multiple obstacles of type D.

The curves defined by multiple obstacles of type D all start at $(0, -\pi)$, as in Fig. 8 which shows an instance with two obstacles defining the constraint curves γ_1 and γ_2. These curves can be ordered by their intersections with a horizontal line $\beta = -\pi + \epsilon$ for small enough $\epsilon >$

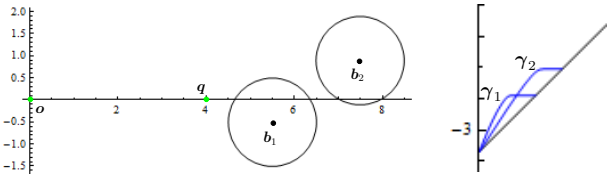

Fig. 8. Two constraint curves γ_1 and γ_2, due to obstacles $\boldsymbol{b}_1$ and $\boldsymbol{b}_2$, respectively, start at the lowest point $(0, -\pi)$ of $\mathcal{D}^-$.

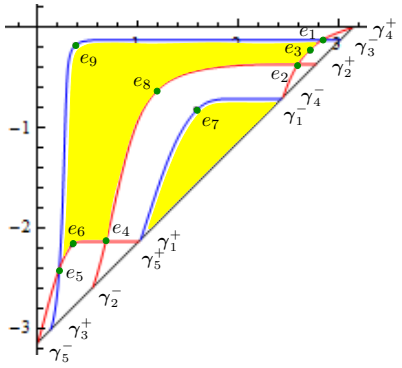

Fig. 9. Shaded regions in the C-space represent all collision-free paths for the environment in Fig. 6(a).

0. Apply Theorem 5, we infer that the α value increase with the x-coordinates of the obstacles. Consequently, the curve γ_i lies to the right of the curve γ_j in $\mathcal{D}^-$ if $\boldsymbol{b}_i$ has a larger x-coordinate than $\boldsymbol{b}_j$ does. In Fig. 8, γ_2 lies to the right of γ_1. All the curves of type D are thus ordered.

The constraint curves induced by type C obstacles all end at the point $(\pi, 0)$. Similarly, these curves appear in the status in the decreasing order of the x-coordinates of the obstacles.

Up to $2n$, where n is the number of obstacles, constraint curves with superscripts, together with the α- and β-axes, are ordered. The array $c[\,]$ can be initialized with a left-to-right scan along the line $\alpha - \beta = \pi$ as follows. We let $c[0]$ to be the number of obstacles of type B. These obstacles are the only ones that define curves to exclude the point $(0, -\pi)$. If the kth scanned curve has superscript '$-$', set $c[k] \leftarrow c[k-1]+1$. If the curve has superscript '$+$', set $c[k] \leftarrow c[k-1]-1$.

Table I details sweeping of the C-space in Fig. 9. Intervals on the sweep line are represented by their left bounding curves. The initial sweep line status is described in the second row. From $c[6] = 0$ we see that the region right above the 6-th segment is collision free.

Every row starting at the third one represents the updated status immediately after an event. To illustrate, the event $\boldsymbol{e}_1$ is due to an intersection between γ_3^-

i	1	2	3	4	5	6	7	8	9	10	11
$s_i, c[i]$	y-axis, 1	$\gamma_5^-, 2$	$\gamma_3^+, 1$	$\gamma_2^-, 2$	$\gamma_5^+, 1$	$\gamma_1^+, 0$	$\gamma_1^-, 1$	$\gamma_4^-, 2$	$\gamma_2^+, 1$	$\gamma_3^-, 2$	$\gamma_4^+, 1$
$\boldsymbol{e}_1$										$\gamma_4^+, 0$	$\gamma_3^-, 1$
$\boldsymbol{e}_2$								$\gamma_2^+, 0$	$\gamma_4^-, 1$		
$\boldsymbol{e}_3$								$\gamma_2^+, 0$			
$\boldsymbol{e}_4$				$\gamma_5^+, 0$	$\gamma_2^-, 1$						
$\boldsymbol{e}_5$		$\gamma_3^+, 0$	$\gamma_5^-, 1$								
$\boldsymbol{e}_6$		$\gamma_3^+, 0$									
$\boldsymbol{e}_7$					$\gamma_2^-, 1$						
$\boldsymbol{e}_8$		$\gamma_3^+, 0$									
$\boldsymbol{e}_9$	y-axis, 1										

TABLE I

EXECUTION OVER THE C-SPACE IN FIG. 9. BLANK ENTRIES ARE THE SAME AS IN THE ROWS IMMEDIATELY ABOVE.

and γ_4^+, which bound the tenth segment. After the intersection, the two curves switching their positions. The obstacles $\boldsymbol{b}_3$ and $\boldsymbol{b}_1$ will not collide with paths in the region bounded by γ_2^+ and γ_4^-.

The event $\boldsymbol{e}_3$ happens at an extremum point on the curve γ_4. In the previous row labeled by $\boldsymbol{e}_2$, γ_4^- and γ_4^+ are next to each other. At $\boldsymbol{e}_3$, the two intervals left-bounded by them along with the preceding interval left-bounded by γ_2^+ are merged into one labeled by γ_2^+. The region immediately above the segment is collision free.

When the sweep finishes, the set of collision-free paths for the sphere is the union of the two shaded open regions shown in Fig. 9.

The plane sweep algorithm does not explicitly construct the constraint curves which do not have algebraic forms. Efficient numerical subroutines have been designed to a) locate a point on a constraint curve given an α or β value; b) compute the starting, ending, and connection points on a constraint curve; c) find the extremum point on a constraint curve; and d) intersect two constraint curves. These subroutines employ bisection or gold section search [9], by exploiting the monotonicity of trajectories as stated in Theorems 4 and 5.

Under a specified accuracy, a call of any numerical subroutine above takes constant time. Then, the running time of the sweep line algorithm for n obstacles is easily analyzed to be $O((n+n_e)\log n)$, where n_e is the number of events (which is $O(n^2)$ in the worst case).

F. Discussion

To have a good clearance from the obstacles, we may pick a point (α, β) that lies close to the center of a region of collision-free trajectories in D^-. Compute the velocities $(\boldsymbol{v}_0, \boldsymbol{\omega}_0)$ from α and β.

Though presented for vertical line obstacles, the algorithm trivially extends to vertical cylindrical obstacles. Extension of the algorithm to polyhedral or other generally shaped obstacles needs further investigation.

The presented work introduces a new way of path planning which takes advantage of sliding under friction. To apply this technique to navigation by spherical robots, two issues await investigation. First, non-uniform mass distribution of such a robot complicates the angular inertial matrix to change dynamic equations significantly. Second, actuation to generate a specified initial motion can be quite challenging.

REFERENCES

[1] S. Bhattacharya and S. K. Agrawal. "Spherical rolling robot: a design and motion planning studies," *IEEE Trans. on Robot. Automat.*, vol. 16, pp. 835–839, 2000.

[2] A. Bicchi, A. Balluchi, D. Prattichizzo, and A. Gorelli. "Introducing the spherical: An experimental testbed for research and teaching in non-holonomy," in *Proc. IEEE Int. Conf. Robot. Autom.*, pp. 2620–2625, 1997.

[3] M. de Berg, M. van Kreveld, M. Overmars, and O. Schwarzkopf. *Computational Geometry: Algorithms and Applications*, 3rd edition, Springer-Verlag, 2008.

[4] T. H. Cormen, C. E. Leiserson, R. L. Rivest, and C. Stein. *Introduction to Algorithms*, 3rd edition, The MIT Press, 2009.

[5] Z. Li and J. Canny. "Motion of two rigid bodies with rolling constraint," *IEEE Trans. on Robot. Automat.*, vol. 6, pp. 72, 1990.

[6] W. C. Marlow. *The Physics of Pocket Billiards*, Marlow Advanced Systems Technologies, 1994.

[7] R. Mukherjee, M. A. Minor, and J. T. Pukrushpan. "Motion planning for a spherical mobile robot: Revising the classcial ball-plate problem," *Trans. of ASME*, vol. 124, pp. 502–511, 2002.

[8] A. Nakashima, K. Nagase, and Y. Hayakawa. "Control of a sphere rolling on a plane with constrained rolling motion," in *Proc. IEEE Conf. Decision and Control*, 2005, pp. 1445–1452.

[9] W. H. Press, S. A. Teukolsky, W. T. Vetterling, and B. P. Flannery. *Numerical Recipes in C++: The Art of Scientific Computing*, 2nd edition, Cambridge University Press, 2002.

[10] D. D. Sleator and R. E. Tarjan. "Self-adjusting binary search trees," *J. ACM*, vol. 32, pp. 652–686, 1985.

[11] M. Svinin and S. Hosoe. "On motion planning for ball-plate systems with limited contact area," in *Proc. IEEE Int. Conf. Robot. Autom.*, 2007, pp. 1820–1824.